

Entropy generation analysis for convective flow of aqua Ag-CuO hybrid nanofluid adjacent to a warmed down-pointing rotating vertical cone

Hamza Berrehal

Department of Physics, Exact Science Faculty, Constantine 1 University, Constantine, Algeria

Roshanak Karami and Saeed Dinarvand

Department of Mechanical Engineering, Islamic Azad University, Central Tehran Branch, Tehran, Iran

Ioan Pop

Department of Mathematics, Babes-Bolyai University, Cluj-Napoca, Romania, and

Ali Chamkha

Faculty of Engineering, Kuwait College of Science and Technology, Doha, Kuwait

Abstract

Purpose – This paper aims to study numerically the flow, heat transfer, and entropy generation of aqueous copper oxide-silver hybrid nanofluid over a down-pointing rotating vertical cone, with linear surface temperature (LST) and linear surface heat flux (LSHF), in the presence of a cross-magnetic field. In industrial applications, such as oil and gas plants, food industries, steel factories and nuclear packages, the real bodies may contain nonorthogonal walls and variable cross-section three-dimensional forms which this issue can clarify the importance of selective geometry in the present research.

Design/methodology/approach – The mass-based scheme is accomplished for the simulation, and the entropy generation and Bejan number will be analyzed in conjunction with the aforementioned model. It has been hypothesized that two types of boundary conditions (LST and LSHF) as well as five nanoparticle shapes (sphere, brick, cylinder, platelet and disk) present a collection of crucial results. The overseeing PDEs are changed over completely to the dimensionless ODEs, and these are solved by Runge-Kutta-Fehlberg approach combined with a shooting methodology for certain values of physical parameters.

Findings – Subsequent to the fantastic compromise of the computational outcomes with past reports, the outcomes are introduced to conduct the investigation of the hydrodynamics/thermal boundary layers, the skin friction and the Nusselt number, as well as entropy generation and Bejan number. A state of hybrid nanofluid, which exhibits a remarkable increase in heat transfer in comparison to the states of mono-nanofluid and regular fluid, has been found to have the highest Nusselt number; however, the skin friction values should always be taken into account and managed. The entropy generation improves with the mass of the second nanoparticle (silver), while the opposite pattern is exhibited for the Bejan number. Furthermore, the lowest value of entropy generation number belongs to the cylindrical shape of nanoparticles in the LST case. In final,



a significant accomplishment of the current study is the accurate output of the mass-based scheme for an entropy analysis problem.

Originality/value – To the best of the authors' knowledge, for the first time, in this study, a new development of natural convective flow of a hybrid nanofluid about the warmed (LST and LSHF) and down-pointing rotating vertical cone by the mass-based algorithm has been presented. The applied methodology considers the masses of base fluid (water) and nanoparticles (Ag and CuO) as an alternative to the first and second nanoparticles volume fraction. Indeed, the combination use of the Tiwari–Das nanofluid model and the mass-based hybridity algorithm for the entropy generation analysis can be the main novelty of this work.

Keywords Entropy generation analysis, Bejan number, Hybrid nanofluid, Down-pointing rotating vertical cone, Mass-based scheme

Paper type Research paper

Nomenclature

- B = strength of magnetic field;
 Be = Bejan number;
 Br = rotational Brinkman number;
 C_f = skin friction coefficient;
 C_p = specific heat at constant pressure;
 F = tangential velocity;
 G = swirl velocity;
 Gr = Grashof number;
 H = temperature;
 k = thermal conductivity;
 m = mass;
 N_G = entropy generation number;
 Nu = Nusselt number;
 M = magnetic parameter;
 Pr = Prandtl number;
 Re = Reynolds number;
 \dot{S}_{gen}'' = actual entropy generation rate;
 \dot{S}_0'' = characteristic entropy generation rate;
 T = temperature of hybrid nanofluid;
 U = reference velocity;
 u = x -direction velocity;
 v = y -direction velocity; and
 w = θ -direction velocity.

Greek symbols

- α = thermal diffusivity;
 β = thermal expansion coefficient;
 ε = parameter related to spin;
 ϕ = nanoparticle volume concentration;
 γ = half of vertex angle;
 μ = dynamic viscosity;
 ρ = density;
 ρC_P = volumetric heat capacity;
 σ = electrical conductivity;
 τ = shear stress;

Φ = viscous dissipation function;
 Ω = angular velocity of the cone; and
 ψ = dimensionless stream function.

Subscripts

∞ = ambient condition;
 f = base fluid;
 nf = mono-nanofluid;
 hnf = hybrid nanofluid;
 s = solid;
 w = surface of the sheet;
1 = first nanoparticle (copper oxide); and
2 = second nanoparticle (silver).

Superscript

' = differentiation with respect to y ;

1. Introduction

In precursor thermal engineering schemes, the outcomes of many experimental and theoretical inquiries manifest the amplification of thermal conductivity with the suspension of solid particles in the regular heat transfer base fluids (Sreedevi *et al.*, 2020; Waini *et al.*, 2021). Nanoparticles (solid particles in sizes of 1–100 nm) are made of metals, carbides, oxides and carbon nanotubes. Ethylene, oil, water and many others are commonly taken as base fluids. Indeed, the nanofluids consist of a mixture of nanoparticles and base materials with a homogenous ratio. The size and shape of such nanoparticles accredit the heat transfer assessment of nanofluids (Tamim *et al.*, 2014). The fluid with the suspension of nanoparticles is explored in various applications, such as cooling and heating phenomenon, nuclear sciences, plasma physics, energy enhancement and fission and fusion processes. Hybrid nanofluids are the combination of two different nanosized particles of metals or nonmetals in the regular base liquids (Agrawal *et al.*, 2021; Berrehal *et al.*, 2022; Ramzan *et al.*, 2022b; Ramzan *et al.*, 2023). These have some positive influences for high performance and cost optimization in thermal engineering packages. Better thermophysical properties of hybrid nanofluids, such as dynamic viscosity, thermal conductivity and density can be achieved by opting the appropriate base fluids as well as solid particles (Jaballah *et al.*, 2019; Afshari *et al.*, 2021; Dinarvand, 2009; Shaheen *et al.*, 2023). Hybrid nanofluids could be used in the following ways: biomedical, sunlight-based energy applications, acoustics, microfluid, miniature electrical, maritime designs, protection, further developed heat exchangers and numerous others (Dinarvand *et al.*, 2022c; Ramzan *et al.*, 2022a; Yazdi *et al.*, 2014; Hoseininejad *et al.*, 2021). A useful package of references about single nanofluid, hybrid nanofluid, their synthesis, their comparison in properties and so on have been presented with numbers (Jana *et al.*, 2007; Li *et al.*, 2021; Menni *et al.*, 2020; Sidik *et al.*, 2017) that easily readers can check and compare these two kinds of working fluid.

For a vertical rotating body that is heated, centrifugal force will appear and act with the forces of buoyancy and Lorentz. Rotational manner of body creates a radially outward motion for the liquid particles. Besides, there is a tangential flow in this problem. Some of the researchers have studied and analyzed this geometry, such as Ozturk and Ece(1995, 1999), Bayram and Ece(2002), Beg *et al.* (2016) and Ozturk (2005). Ozturk (2005) has investigated the laminar mixed convection flow on a rotation spherical body. He also considered the effect of the magnetic field to demonstrate that the heat transfer on upstream face increases

with the magnetic field. In an interesting study, the unsteady convective flow about a rotational cone was explored by Takhar *et al.* (2003). They considered a transverse magnetic field and also a time-dependent angular velocity for their problem. The flow and heat transfer characteristics were explored and analyzed in this work. Besides, Chamkha and Al-Mudhaf (2005) have investigated the heat and mass transfer of flow about a rotational cone with absorption and generation effects. Besides, some other works on the flow and heat transfer over cones can be found in the references (Chandra Sekar Reddy *et al.*, 2022; Reddy *et al.*, 2023; Reddy *et al.*, 2018).

Regarding the above investigations, no one has ever attempted to study the free-convective flow of an electrically conducting hybrid nanofluid adjacent to a down-pointing rotating vertical cone in the presence of a transverse magnetic field using a new mass-based scheme (Yazdi *et al.*, 2014; Dinarvand *et al.*, 2022a; Dinarvand and Mahdavi Nejad, 2022). The mass-based hybridity model is a new approach for modeling hybrid nanofluids, which differs from the traditional fraction-based method. In the fraction-based method, the properties of the nanofluid are calculated based on the volume fractions of the base fluid and nanoparticles. However, the mass-based hybridity model takes into account the mass fractions of the base fluid and nanoparticles. As a result, it can better capture the effects of the nanoparticles on the overall properties of the nanofluid. In former methods of modeling by the fraction-based scheme, one cannot see directly the effect of the first and second nanoparticle masses on various quantities of problem. Therefore, this can be a serious motivation for authors to apply the mass-based scheme for the present problem to get a set of interesting and more comprehensible results. The major path contains to solve numerically and analyze the present problem by considering silver (Ag) and copper oxide (CuO) as nanoparticles in water (base liquid). The Runge–Kutta–Fehlberg method and a shooting scheme are used to solve the resulting similarity ODEs with relevant boundary conditions. In addition, the effect of the emerging parameters on the hybrid nanofluid flow and heat transfer features of the current problem is illustrated and discussed in graphical and tabular form following a good agreement between our numerical results and those of previous studies. In addition, the Bejan number and the entropy generation number would be calculated for a comprehensive analysis of entropy generation.

2. Natural convective flow of hybrid nanofluid and problem details

According to Figure 1, consider the steady natural convective boundary layer flow along a warmed and down-pointing rotating vertical cone in a hybrid nanofluid in the presence of a transverse magnetic field normal to the body.

According to Tiwari–Das model (Tiwari and Das, 2007), the continuity, momentum and energy equations (Ece, 2006; Dinarvand and Pop, 2017) of present hybrid nanofluid flow are as follows:

$$\frac{\partial}{\partial x^*}(r^*u^*) + \frac{\partial}{\partial y^*}(r^*v^*) = 0, \quad (1)$$

$$\rho_{lmf} \left(u^* \frac{\partial u^*}{\partial x^*} + v^* \frac{\partial u^*}{\partial y^*} - \frac{w^{*2}}{x^*} \right) = \mu_{lmf} \frac{\partial^2 u^*}{\partial y^{*2}} + (\rho\beta)_{lmf} g \cos \gamma (T - T_0) - \sigma B^2 u^*, \quad (2)$$

$$\rho_{lmf} \left(u^* \frac{\partial w^*}{\partial x^*} + v^* \frac{\partial w^*}{\partial y^*} + \frac{u^* w^*}{x^*} \right) = \mu_{lmf} \frac{\partial^2 w^*}{\partial y^{*2}} - \sigma B^2 w^*, \quad (3)$$

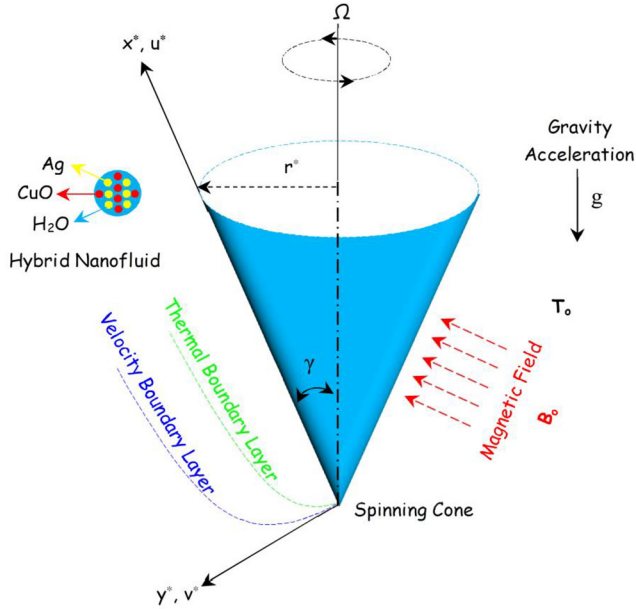


Figure 1. Schematic of hybrid nanofluid natural convection, nanoparticles, base fluid and magnetic field effect

Source: Figure by authors

$$(\rho C_p)_{hnf} \left(u^* \frac{\partial T}{\partial x^*} + v^* \frac{\partial T}{\partial y^*} \right) = k_{hnf} \frac{\partial^2 T}{\partial y^{*2}}, \quad (4)$$

The prescribed temperature or heat flux on the cone can be presented in the below form:

$$T(x^*, 0) = A(x^*) \quad \text{or} \quad -k \frac{\partial T}{\partial y^*} \Big|_{y^*=0} = C(x^*), \quad (5)$$

and hydrodynamics boundary conditions are:

$$u(x^*, 0) = 0, \quad v(x^*, 0) = 0, \quad w(x^*, 0) = r^*. \quad (6)$$

In the above relations, the electrical conductivity has been shown with σ , the magnetic field has been presented with $B = B_0 b(x)/(r\sqrt{1-r'^2})$ and vertex angle has been shown with γ . Moreover, thermophysical properties of hybrid nanofluid, such as k_{hnf} , μ_{hnf} , β_{hnf} and ρ_{hnf} have been listed in Table 1. Figure 2 has been presented as the shape factor of nanoparticles applied in this research. As it is observable in Table 1, the effective viscosity needs two constants to be evaluated; therefore, Table 2 is presented to list these values. Finally, to complete the governing equations with all parameters and properties, we have Table 3 for the mass-based algorithm. Physical properties of water, copper oxide (CuO) and silver (Ag) are shown in Table 4.

Nondimension variables applied in the analysis are defined as (Ece, 2006; Dinarvand and Pop, 2017):

$$\begin{aligned} x &= \frac{x^*}{L}, & y &= \frac{y^*}{L} Gr^{1/4}, & r &= \frac{r^*}{L}, \\ u &= \frac{u^*}{U}, & v &= \frac{v^*}{U} Gr^{1/4}, & w &= \frac{w^*}{\Omega L}, & \Theta &= \frac{T - T_0}{T_r - T_0}, \end{aligned} \quad (7)$$

Prandtl and Grashof numbers are as:

$$U = [g \cos \gamma \beta L (T_r - T_0)]^{1/2}, \quad Gr = \left(\frac{UL}{\nu} \right)^2, \quad Pr = \frac{\nu}{\alpha}. \quad (8)$$

Considering the above relations, one can change the equations to the below form:

$$\frac{\partial}{\partial x}(ru) + \frac{\partial}{\partial y}(rv) = 0, \quad (9)$$

$$u \frac{\partial u}{\partial x} + v \frac{\partial u}{\partial y} - \frac{Re^2 r'}{Gr r} w = \frac{\rho_f}{\rho_{hmf}} \left(\frac{\mu_{hmf}}{\mu_f} \frac{\partial^2 u}{\partial y^2} + \frac{(\rho\beta)_{hmf}}{(\rho\beta)_f} \Theta + M\Lambda^2 u \right), \quad (10)$$

$$u \frac{\partial w}{\partial x} + v \frac{\partial w}{\partial y} - uw \frac{r'}{r} = \frac{\rho_f}{\rho_{hmf}} \left(\frac{\mu_{hmf}}{\mu_f} \frac{\partial^2 w}{\partial y^2} - M\Lambda^2 w \right), \quad (11)$$

$$u \frac{\partial \Theta}{\partial x} + v \frac{\partial \Theta}{\partial y} = \frac{1}{Pr} \frac{(\rho C_p)_f}{(\rho C_p)_{hmf}} \frac{k_{hmf}}{k_f} \frac{\partial^2 \Theta}{\partial y^2}, \quad (12)$$

Properties	formulation
Density	$\rho_{hmf} = (1 - \varphi)\rho_f + \varphi\rho_s$
Heat capacitance	$(\rho c_p)_{hmf} = (1 - \varphi)(\rho c_p)_f + \varphi(\rho c_p)_s$
Thermal expansion coefficient	$(\rho\beta)_{hmf} = \varphi_1(\rho\beta)_1 + \varphi_2(\rho\beta)_2 + (1 - \varphi)(\rho\beta)_f$
Dynamic viscosity	Spherical nanoparticles $\mu_{hmf} = \frac{\mu_f}{(1 - \varphi)^{2.5}}$
	Nonspherical nanoparticles $\mu_{hmf} = \mu_f(1 + A\varphi + B\varphi^2)$
Thermal conductivity	$\frac{k_{hmf}}{k_{nf}} = \frac{k_{s2} + (n - 1)k_{nf} - (n - 1)\varphi_2(k_{nf} - k_{s2})}{k_{s2} + (n - 1)k_{nf} + \varphi_2(k_{nf} - k_{s2})}$
	$\frac{k_{nf}}{k_f} = \frac{k_{s1} + (n - 1)k_f - (n - 1)\varphi_1(k_f - k_{s1})}{k_{s1} + (n - 1)k_f + \varphi_1(k_f - k_{s1})}$

Source: Table by authors

Table 1. Hybrid nanofluids relations including density, heat capacitance, thermal expansion coefficient, dynamic viscosity and thermal conductivity (Dinarvand *et al.*, 2022a; Dinarvand and Mahdavi Nejad, 2022; Tiwari and Das, 2007; Devi and Devi, 2016)

with

$$\begin{aligned} u(x, 0) &= 0, & u(x, \infty) &= 0, \\ w(x, 0) &= r, & w(x, \infty) &= 0, \\ \Theta(x, 0) &= a(x) \quad \text{or} \quad \left. \frac{\partial \Theta}{\partial y} \right|_{y=0} = -c(x), & \Theta(x, \infty) &= 0 \end{aligned} \tag{13}$$

In above, $a(x) = (A(x) - T_0)/(T_r - T_0)$ and $c(x) = Gr^{-1/4}LC(x)/k(T_r - T_0)$, the rotational Reynolds number Re and the magnetic field function Λ are defined as:

$$Re = \frac{\Omega L^2}{\nu_f}, \quad \Lambda = \frac{b(x)}{r\sqrt{1 - r'^2}}, \tag{14}$$

where $b(x)$ is a function proportional to x . The M denotes to the magnetic parameter and is defined as:

$$M = \frac{\sigma B_0^2 L}{U \rho_f}. \tag{15}$$

One can present stream function ψ as follows:





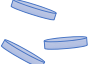
$$ru = \frac{\partial \psi}{\partial y} \quad \text{and} \quad rv = -\frac{\partial \psi}{\partial x} \tag{16}$$

with variables as:

$$\psi(x, y) = xrF(y), \quad w = rG(y), \quad \Theta = xH(y), \tag{17}$$

Now, the equations (9)–(12) will be reduced to:

$$A_0 F'''(y) + 2F(y)F''(y) - [F'(y)]^2 + \varepsilon[G(y)]^2 - A_1 M F'(y) + A_2 H(y) = 0, \tag{18}$$

Nanoparticle shapes	Sphere	Brick	Cylinder	Platelet	Disk
Shape structure					
ψ	1	0.81	0.62	0.52	0.36
n	3	3.7	4.8	5.7	8.3

Source: Timofeeva *et al.* (2009), Sheikholeslami and Shamlooei (2017)

Figure 2.
The values of ψ and n for nanoparticles

Table 2.
The constants in the effective viscosity relation (Timofeeva *et al.*, 2009; Sheikholeslami and Shamlooei, 2017)

Model	Bricks shape	Cylinder shape	Platelets shape	Disk shape
A	1.9	13.5	37.1	14.6
B	471.4	904.4	612.6	123.3

Source: Table by authors

Title	Mathematical relations
Equivalent density	$\rho_s = \frac{(\rho_1 \times w_1) + (\rho_2 \times w_2)}{w_1 + w_2}$
Equivalent specific heat of nanoparticles at constant pressure	$(C_p)_s = \frac{((C_p)_1 \times w_1) + ((C_p)_2 \times w_2)}{w_1 + w_2}$
Solid volume fraction of first nanoparticle	$\varphi_1 = \frac{\frac{w_1}{\rho_1}}{\frac{w_1}{\rho_1} + \frac{w_2}{\rho_2} + \frac{w_f}{\rho_f}}$
Solid volume fraction of second nanoparticle	$\varphi_2 = \frac{\frac{w_2}{\rho_2}}{\frac{w_1}{\rho_1} + \frac{w_2}{\rho_2} + \frac{w_f}{\rho_f}}$
Equivalent volume fraction of nanoparticles	$\varphi = \varphi_1 + \varphi_2 = \frac{\frac{w_1 + w_2}{\rho_s}}{\frac{w_1 + w_2}{\rho_s} + \frac{w_f}{\rho_f}}$

Table 3. The relations for new algorithm based on masses (Yazdi *et al.*, 2014; Dinarvand *et al.*, 2022a; Dinarvand and Mahdavi Nejad, 2022)

Note: To obtain the final relations of hybrid nanofluid properties, the mass-based definitions presented in Table 4 [$\rho_s, (C_p)_s, \varphi_1, \varphi_2$ and φ] should be substituted into the original relations presented in Table 1
Source: Table by authors

Thermophysical properties	Water	Copper oxide (CuO)	Silver (Ag)
C_p (J/kgK)	4179	531.8	235
ρ (kg/m ³)	997.1	6320	10500
k (W/mk)	0.613	76.5	429
$\beta \times 10^5$ (1/K)	21	1.8	1.3
Particle size (nm)	–	–	2–5

Table 4. Physical properties of water, copper oxide (CuO) and silver (Ag) (Hayat and Nadeem, 2017; Alarabi *et al.*, 2021)

Source: Table by authors

$$A_0 G''(y) + 2 \left| \frac{F(y)}{F'(y)} \frac{G(Y)}{G'(y)} \right| - A_1 M G(y) = 0, \tag{19}$$

$$A_3 H''(y) + \text{Pr} [2F(y)H'(y) - F'(y)H(y)] = 0. \tag{20}$$

$$A_0 = \left(1 - \frac{\frac{w_1 + w_2}{\rho_s}}{\frac{w_1 + w_2}{\rho_s} + \frac{w_f}{\rho_f}} \right)^{-2.5} \left(1 - \frac{\frac{w_1 + w_2}{\rho_s}}{\frac{w_1 + w_2}{\rho_s} + \frac{w_f}{\rho_f}} + \frac{\frac{w_1 + w_2}{\rho_s}}{\frac{w_1 + w_2}{\rho_s} + \frac{w_f}{\rho_f}} \frac{\rho_s}{\rho_f} \right)^{-1},$$

$$A_1 = \left(1 - \frac{\frac{w_1+w_2}{\rho_s}}{\frac{w_1+w_2}{\rho_s} + \frac{w_f}{\rho_f}} + \frac{\frac{w_1+w_2}{\rho_s} \frac{\rho_s}{\rho_f}}{\frac{w_1+w_2}{\rho_s} + \frac{w_f}{\rho_f}} \right)^{-1},$$

$$A_2 = \left(1 - \frac{\frac{w_1+w_2}{\rho_s}}{\frac{w_1+w_2}{\rho_s} + \frac{w_f}{\rho_f}} + \frac{\frac{w_1+w_2}{\rho_s} \frac{(\rho\beta)_s}{(\rho\beta)_f}}{\frac{w_1+w_2}{\rho_s} + \frac{w_f}{\rho_f}} \right) \left(1 - \frac{\frac{w_1+w_2}{\rho_s}}{\frac{w_1+w_2}{\rho_s} + \frac{w_f}{\rho_f}} + \frac{\frac{w_1+w_2}{\rho_s} \frac{\rho_s}{\rho_f}}{\frac{w_1+w_2}{\rho_s} + \frac{w_f}{\rho_f}} \right)^{-1},$$

$$A_3 = \frac{k_{hmf}}{k_f} \left(1 - \frac{\frac{w_1+w_2}{\rho_s}}{\frac{w_1+w_2}{\rho_s} + \frac{w_f}{\rho_f}} + \frac{\frac{w_1+w_2}{\rho_s} \frac{\rho_s}{\rho_f}}{\frac{w_1+w_2}{\rho_s} + \frac{w_f}{\rho_f}} \right)^{-1}.$$

Here, the spin parameter is $\varepsilon = (\text{Re} \sin \gamma)^2 / Gr$. The equations (13) also transform to following form:

$$F(0) = 0, \quad F'(0) = 0, \quad G(0) = 1, \quad H(0) = \frac{a(x)}{x} \quad \text{or} \quad H'(0) = -\frac{c(x)}{x} \quad (21)$$

$$F'(\infty) = 0, \quad G(\infty) = 0, \quad H(\infty) = 0. \quad (22)$$

Here, the prime implies differentiation with respect to y functions associated with the heat transfer boundary conditions given by equation (22) should be equal to a constant to enable a similarity solution. This condition needs the functions $a(x)$ and $c(x)$ to be proportional to x . The thermal boundary conditions can be stated as:

$$\text{LST Case with } H(0) = 1 \quad \text{or} \quad \text{LSHF Case with } H'(0) = -1 \quad (23)$$

An important point to note is that, this research transforms to works by Ece (2006) and Dinarvand and Pop(2017) for a viscous fluid when $\phi = 0$ (regular fluid).

The skin friction coefficients C_f and the local Nusselt number Nu are as below:

$$C_f = \frac{2\tau_w}{\rho_f U^2}, \quad Nu = \frac{Lq_w}{k_f(T_w - T_\infty)}, \quad (24)$$

where

$$\tau_w = \mu_{hmf} \left(\frac{\partial u^*}{\partial y^*} \right)_{y^*=0}, \quad q_w = -k_{hmf} \left(\frac{\partial T}{\partial y^*} \right)_{y^*=0} \quad (25)$$

Using the dimensionless transformations (7)–(8) and (17), one can write:

$$C_f Gr^{1/4} = 2 \left(\frac{\mu_{hmf}}{\mu_f} \right) x F''(0), \quad Nu Gr^{-1/4} = - \left(\frac{k_{hmf}}{k_f} \right) x H'(0). \quad (26)$$

Here, we suggest readers to refer the base and original articles on this problem (Ece, 2001, 1999–2000) to get some information from mathematics details and dimensionless analysis.

3. Entropy generation in framework of the mass-based scheme

The volumetric rate of entropy generation is based on (Bejan, 1979; Mahian *et al.*, 2012):

$$S_{gen}'' = \frac{k_{lmf}}{T_r^2} [\nabla T]^2 + \frac{\mu_{lmf}}{T_r} \Phi + \frac{1}{T_r} [(J - QV) \cdot (E + V \times B)], \quad (27)$$

where

$$[\nabla T]^2 = \left[\left(\frac{\partial T}{\partial x^*} \right)^2 + \left(\frac{\partial T}{\partial y^*} \right)^2 \right], \quad (28)$$

$$\Phi = 2 \left[\left(\frac{\partial u^*}{\partial x^*} \right)^2 + \left(\frac{u^*}{x^*} \right)^2 + \left(\frac{\partial v^*}{\partial y^*} \right)^2 \right] + \left(\frac{\partial w^*}{\partial y^*} \right)^2 + \left(\frac{\partial u^*}{\partial y^*} \right)^2, \quad (29)$$

$$J = \sigma (E + \vec{V} \times \vec{B}). \quad (30)$$

Assume that the electric force [in comparison with $\vec{V} \times \vec{B}$ in equations (26) and (30)] is small and also suppose that the electric current is too larger than QV . Therefore, using the foregoing assumptions, equation (26) can be reduced as:

$$S_G = \frac{k_{lmf}}{T_r^2} \left[\left(\frac{\partial T}{\partial x^*} \right)^2 + \left(\frac{\partial T}{\partial y^*} \right)^2 \right] + \frac{\mu_{lmf}}{T_r} \left\{ 2 \left[\left(\frac{\partial u^*}{\partial x^*} \right)^2 + \left(\frac{u^*}{x^*} \right)^2 + \left(\frac{\partial v^*}{\partial y^*} \right)^2 \right] + \left(\frac{\partial w^*}{\partial y^*} \right)^2 + \left(\frac{\partial u^*}{\partial y^*} \right)^2 \right\}$$

Joule dissipation irreversibility

$$+ \frac{\sigma B_0}{T_r} (u^{*2} + w^{*2}) = 0 \quad (31)$$

The nondimensional form of the entropy generation rate is the entropy generation number (N_G), which denotes the ratio between the actual entropy generation rate (\dot{S}_{gen}) and the characteristic entropy generation rate (\dot{S}_0). The boundary layer variables (16) and (17) and the dimensionless variables of equations (6) and (7) are applied to equation (31); therefore, N_G can be written as:

$$N_G = \frac{\alpha}{Re} (H^2 + Gr^{1/2} H'^2) + \frac{Br}{Re} \left\{ 11F'^2 + Gr^{1/2} (F''^2 + s^2 \sin^2 \gamma G'^2) \right\} + \frac{Br}{s} M (F'^2 + s^2 \sin^2 \gamma G^2), \quad (32)$$

In equation (32), $Br = \mu_f U^2 / K_f \Delta T$ is the rotational Brinkman number, $a = \Delta T / T_r$ is the nondimension temperature difference, $s = \Omega L / U$ is the nondimensional parameter, $Re = \Omega L^2 / \nu_f$ is the rotational Reynolds number and $N_G = \dot{S}_{gen}''' / (K_f \Omega \Delta T / \nu_f T_r)$ is the nondimensional entropy generation rate.

In final, the Bejan number for the foregoing problem can be defined as:

$$Be = \frac{\frac{\alpha}{Re} (H^2 + Gr^{1/2} H'^2)}{\frac{\alpha}{Re} (H^2 + Gr^{1/2} H'^2) + \frac{Br}{Re} \left\{ 11F'^2 + Gr^{1/2} (F'^2 + s^2 \sin^2 \gamma G^2) \right\} + \frac{Br}{s} M (F'^2 + s^2 \sin^2 \gamma G^2)} \quad (33)$$

From equation (33), it is clear that $0 < Be < 1$. When $Be = 0$, the fluid friction and joule dissipation irreversibility overcome entropy generation, when $Be = 1/2$ the portion of the heat transfer irreversibility is equivalent to the sum total of the fluid friction and Joule heating, and when $Be = 1$ the mechanism of irreversibility is dominated by heat transfer influences. A review of entropy generation analysis can be found in Mahian *et al.* (2013).

4. Numerical procedure and validation reports

The governing equations (1)–(4) are transformed to the set of coupled nonlinear ordinary differential equations (18)–(20) using the similarity scheme, which are numerically (by Runge–Kutta–Fehlberg technique) solved for different values of the controlling parameters $w_1, w_2, w_f, n_1, n_2, \varepsilon, M$ and Pr . The problem may be solved twice using step sizes $\Delta\eta$ and $\Delta\eta/2$, and the results can be compared at the mesh locations corresponding to the greater step size to ensure correctness in the solution. The lower step size, however, necessitates a large amount of calculation, and this process must be repeated if the agreement is found to be insufficient. One approach to attempting to address this conundrum is the Runge–Kutta–Fehlberg technique. It has a method to check whether the right step size is being used. Two distinct approximations for the answer are created and contrasted at each stage. The approximation is approved if there is substantial agreement between the two responses. The step size is decreased if there is a discrepancy between the two responses to a given accuracy. The step size is raised if the solutions agree to more significant digits than necessary. In operation, $\eta = \infty$ must be considered by an approximation $\eta = \eta_{max}$, where η_{max} is optional as long as it is chosen great enough so that the solution demonstrates small further change for η greater than η_{max} . To evaluate the accuracy of the present results, the validity of the computational code has been explored for some special cases. Tables 5 and 6 show the values of $F'(0)$ and $-H'(0)$ for rotating cone with the linear surface temperature (LST) and linear surface heat flux (LSHF), respectively, when $w_1 = w_2 = 0$ (for pure water case). In these tables, a comparison is performed with already published results of Ece (2006) that demonstrates a favorable agreement with this work.

5. Results and discussions

5.1 Behavior analysis of hydrodynamics and thermal boundary layers

Here, an analysis for the behavior of the thermal and hydrodynamics boundary layers based on different controlling parameters will be performed and discussed. The tangential velocity profiles $F'(y)$, the swirl velocity profiles $G(y)$ and temperature distribution $H(y)$ about a spinning vertical cone with the LST and LSHF for the various values of the magnetic parameter are demonstrated in Figure 3(a,b). On the presence of a magnetic field, the Lorentz force (a drag-like force) is appeared by the imposition of the transverse magnetic field to the

electrically conducting hybrid nanofluid. The foregoing force has a trend to slow down the flow on the cone surface. Indeed, the magnetic field causes a reduction in the boundary layer thickness which results in a higher velocity gradient on the wall. Consequently, as the shear stress is directly proportional to the velocity gradient (based on Newton’s law of viscosity), the augmentation of the magnetic field causes an increase in the wall’s shear stress. It is worth mentioning, this result is valid for both two cases of LST and LSHF. On the other hand, the resistance induced by the fluid flow is responsible for augmenting the temperature. Indeed, the Lorentz force has a trend to enhance the boundary layer temperature and this means a lower temperature gradient on the wall. According to the first definition of the convective heat transfer coefficient, the temperature gradient has a direct relation with the convective heat transfer coefficient. Finally, from Figure 3(a), the distribution temperature enhances, the temperature gradient reduces and the heat flux of the surface decreases dramatically with augmenting values of the magnetic parameter.

The effect of the different values of rotational parameter ε on the tangential velocity profiles $F'(y)$, the swirl velocity profiles $G(y)$ and temperature distribution $H(y)$ about a spinning cone with LST and also LSHF is shown in Figure 4(a,b). Rotation of the cone intend to enhance the tangential velocity magnitude because of the induced axial flow. Besides, the velocity augmentation due to the body rotation increases convection heat transfer and squeeze the temperature distribution toward the wall. Furthermore, it is obvious that the rotational parameter has a compressing effect on swirl velocity.

Figure 5(a,b) is plotted to analyze the influence of the second nanoparticle mass w_2 on the tangential velocity profiles $F'(y)$, the swirl velocity profiles $G(y)$ and temperature distribution $H(y)$ for two cases of LST and LSHF. An augmentation in hybrid nanofluid tangential velocity is observed with the enhancement in w_2 , although an oppose trend is observable for the swirl velocity profiles. Moreover, the second nanoparticle mass expands the temperature

Table 5.

Values of $F''(0)$ and $-H'(0)$ for rotating cone with LST, and comparison with the results of Ece (2006) for various values of ε , M and Pr for regular fluid ($\phi = w_1 = w_2 = 0$)

ε	M	$F''(0)$				$-H'(0)$			
		$Pr = 1$		$Pr = 10$		$Pr = 1$		$Pr = 10$	
		Ece (2006)	Present	Ece (2006)	Present	Ece (2006)	Present	Ece (2006)	Present
0	5	0.37090	0.370906	0.29345	0.293445	0.40364	0.403652	0.95839	0.958424
	10	0.28500	0.285003	0.24343	0.243348	0.32121	0.321215	0.82300	0.823800
2	5	0.65693	0.656741	0.56901	0.568997	0.43485	0.435816	1.12833	1.128430
	10	0.49307	0.493074	0.44699	0.446976	0.33617	0.336177	0.91826	0.918457

Source: Table by authors

Table 6.

Values of $F''(0)$ and $-H'(0)$ for rotating cone with LSHF, and comparison with the results of Ece (2006) for various values of ε , M and Pr for regular fluid ($\phi = w_1 = w_2 = 0$)

ε	M	$F''(0)$				$-H'(0)$			
		$Pr = 1$		$Pr = 10$		$Pr = 1$		$Pr = 10$	
		Ece (2006)	Present	Ece (2006)	Present	Ece (2006)	Present	Ece (2006)	Present
0	5	0.67482	0.671757	0.30161	0.300212	1.92292	1.916344	1.03217	1.029853
	10	0.60773	0.604952	0.27654	0.275011	2.22496	2.216272	1.15199	1.147534
2	5	0.93347	0.933476	0.54621	0.546180	1.85491	1.854919	0.90700	0.906942
	10	0.80220	0.802209	0.46141	0.461358	2.18032	2.180329	1.06718	1.067010

Source: Table by authors

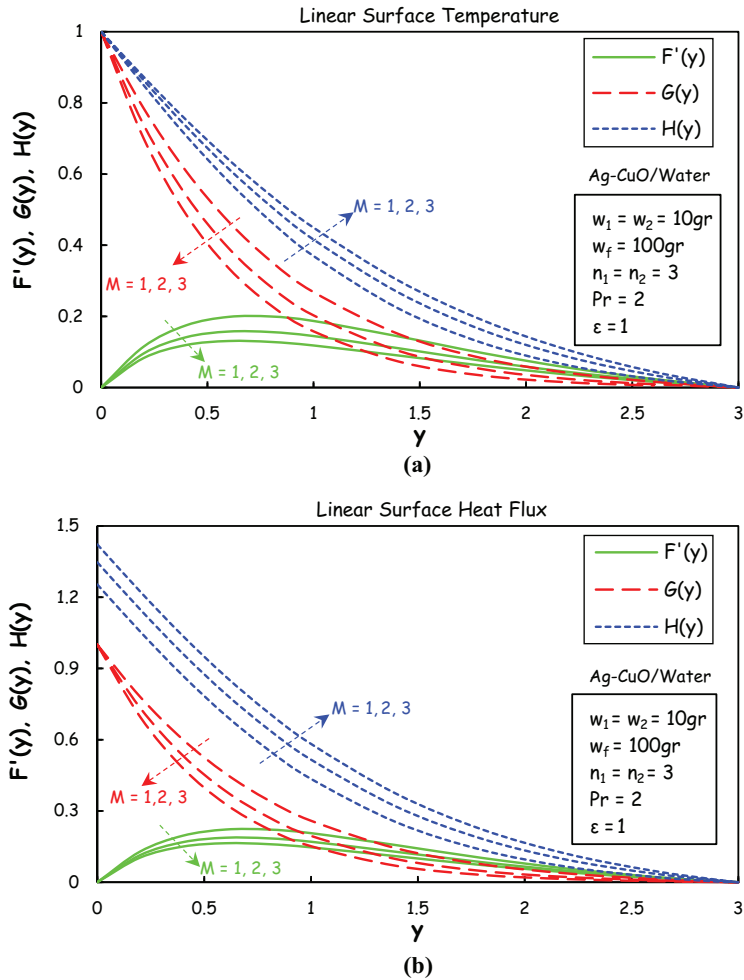
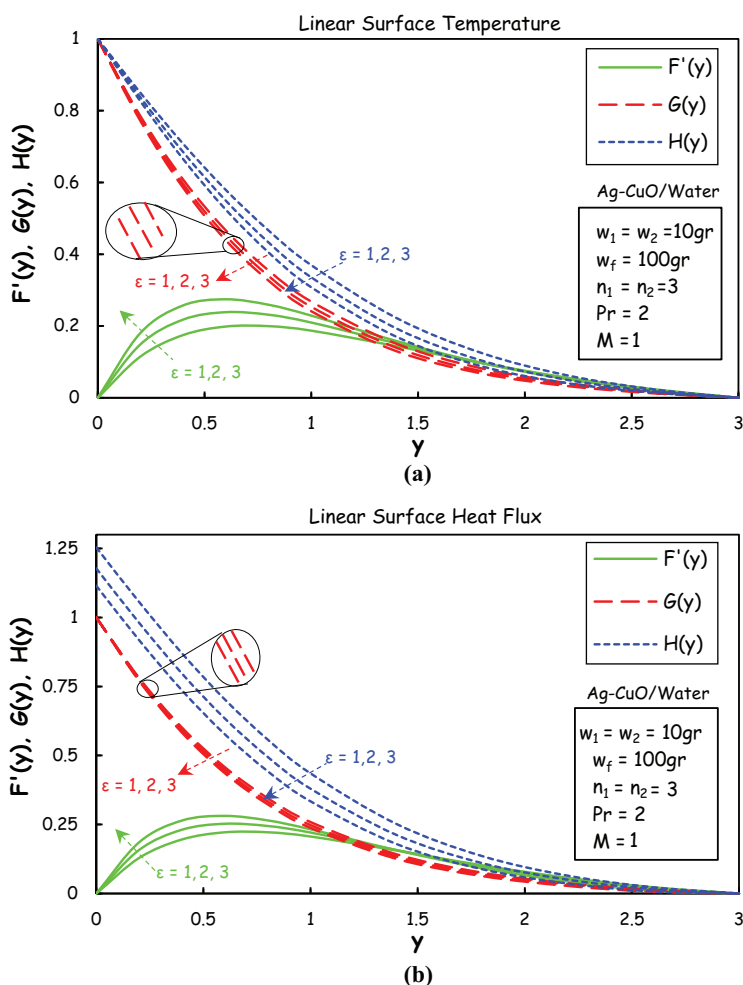


Figure 3. Variation of tangential velocity, swirl velocity and temperature with magnetic parameter

Notes: (a) LST case; (b) LSHF case
Source: Figure by authors

and this increases width in the thermal boundary layer. Besides, the heat transfer characteristics will be affected by this change in the hybrid nanofluid boundary layer.

Figure 6(a,b) shows the influence of the empirical shape factor n on velocities components of tangential and swirl for both two cases of LST and LSHF. This figure demonstrates that cylindrical nanoparticle gives the lowest tangential velocity and highest axial velocity. It means that the velocity gradient on wall for both components of velocities decreases with the empirical shape factor; while this affects dramatically hydrodynamic characteristics of hybrid nanofluid flow. However, one cannot conclude what kind of change will be occurred as other factors, such as effective viscosity, are impressive in hydrodynamic characteristics. Besides, the effect of the empirical shape factor n on the temperature profile



Notes: (a) LST case; (b) LSHF case
Source: Figure by authors

Figure 4. Variation of tangential velocity, swirl velocity and temperature with spin parameter

for both two cases of LST and LSHF is observable in Figure 6(a,b). From this figure, the highest temperature is related to cylindrical nanoparticles and the lowest one belongs to spherical nanoparticles. As in the previous parts, the change of the boundary layer's temperature and its effect on heat transfer were discussed, to avoid repetitive contents, this issue will not be remarked on again, here.

5.2 Skin friction and heat transfer rate

Two parameters of engineering interest are $(1/x)C_f Gr^{1/4}$ and $(1/x)Nu_x Gr^{-1/4}$ which will be calculated and analyzed in this section. Figure 7(a,b) plotted to show $(1/x)C_f Gr^{1/4}$ for two cases of LST and LSHF, when $w_f = 100 \text{ gr}$, $n_1 = n_2 = 3$, $\epsilon = M = 1$ and $Pr = 2$. The results

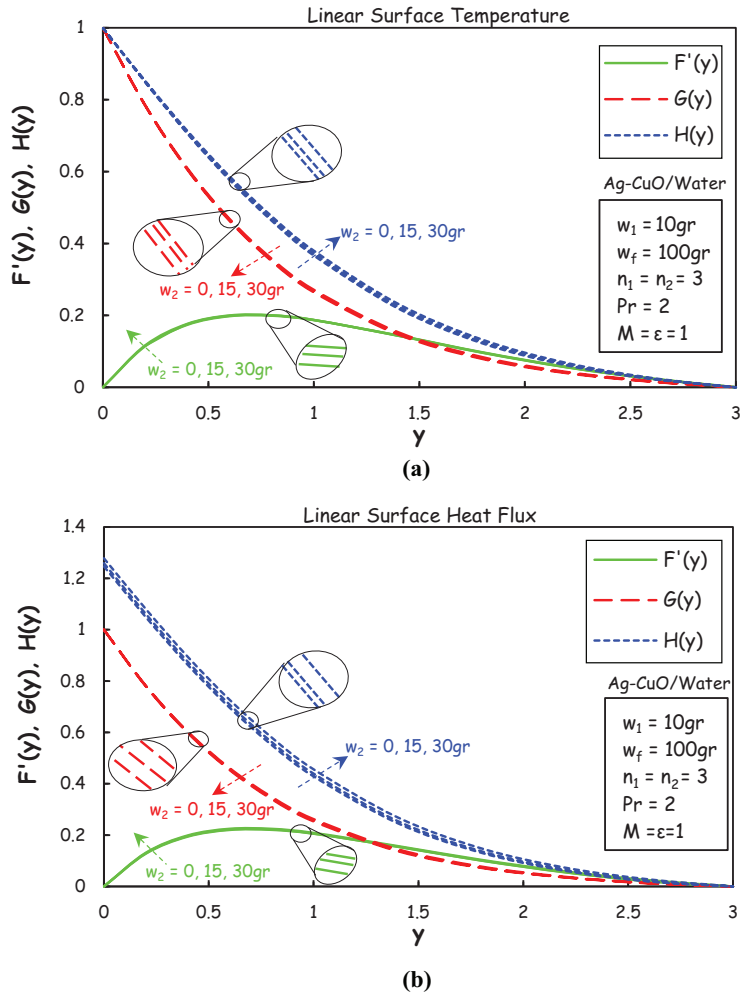
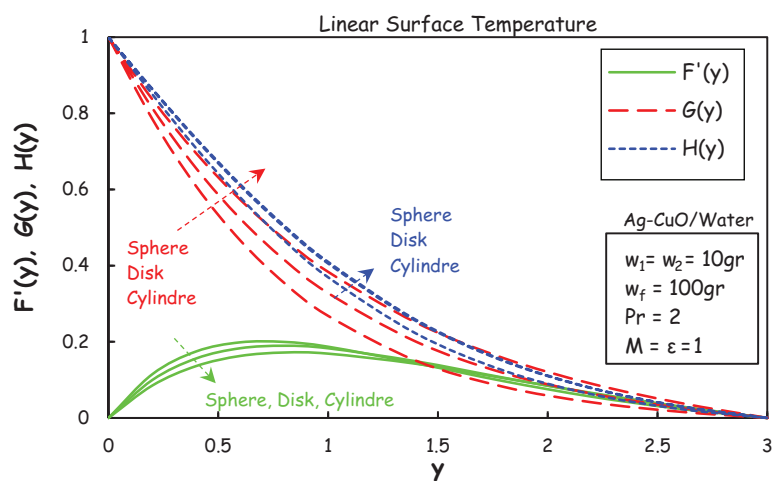


Figure 5.
Variation of tangential velocity, swirl velocity and temperature with second nanoparticle mass

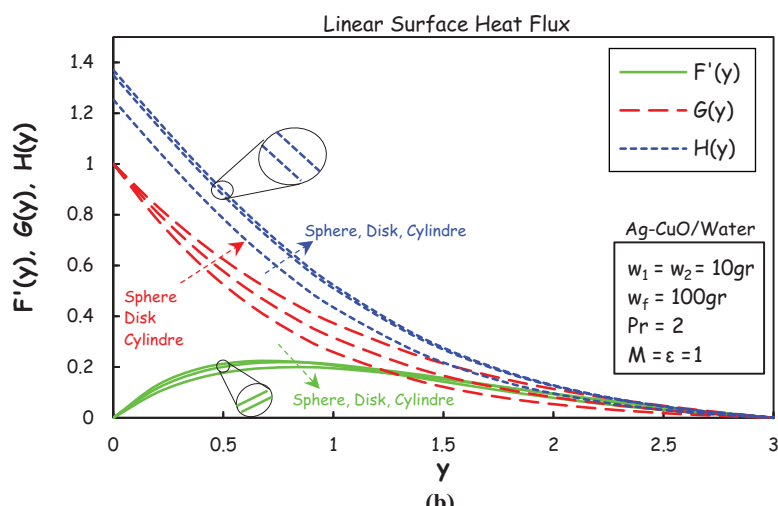
Notes: (a) LST case; (b) LSHF case
Source: Figure by authors

have shown for different kinds of fluids, including the conventional fluid (pure water), single-particle nanofluids (copper oxide/water and silver/water) and double-particle hybrid nanofluids (copper oxide-silver/water), which one can compare the values of skin friction in a glance (see Table 7).

Figure 8(a) demonstrates $(1/x)Nu_xGr^{-1/4}\epsilon$ for different kinds of fluids considering the LST case. Besides, the enhanced Nusselt number percentage of mono-nanofluid and hybrid nanofluid relative to the regular fluid has been shown in the Figure 8(a) that can help readers for better realization of the results. Obviously, for all states both the Nusselt number enhances with the increase in first (copper oxide) and second (silver) nanoparticle masses. Indeed, when the nanoparticles mass enhances, the effective thermal conductivity augments



(a)



(b)

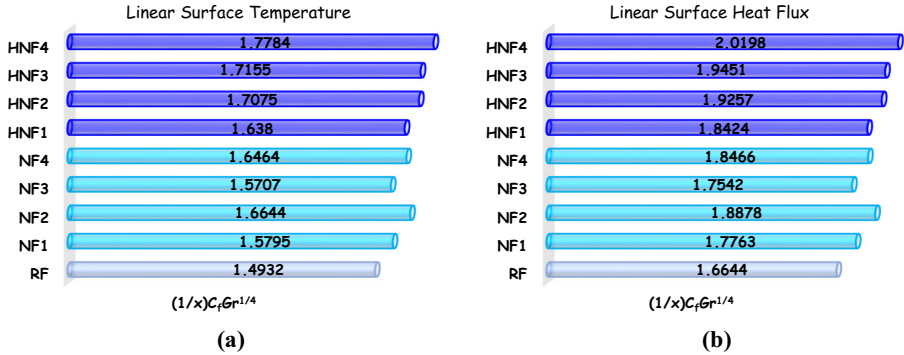
Notes: (a) LST case; (b) LSHF case
Source: Figure by authors

Figure 6. Variation of tangential velocity, swirl velocity and temperature with different shapes of nanoparticle

and this issue affects the heat transfer rate of the working fluid. Figure 8(a) demonstrates $(1/x)Nu_x Gr^{-1/4}$ for different kinds of fluids considering the LST case. Besides, Figure 8(a) shows that hybrid nanofluid and mono-nanofluid have a higher Nusselt number percentage than conventional working liquid, which may assist readers in better comprehending the results. Clearly, as the copper oxide and silver nanoparticle masses rise, so does the Nusselt number for all states. In fact, the issue has an effect on the working fluid's heat transfer rate because an increase in the mass of the nanoparticle increases its effective thermal

conductivity. Importantly, $(1/x)Nu_xGr^{-1/4}$ is too low when only the first nanoparticle is added to the base fluid compared to when only the second nanoparticle is added. Clearly, one can see this with comparison between states of NF1 and NF2 with states of NF3 and NF4. This occurs as according to Table 4, the thermal conductivity of copper oxide is too small in

Figure 7. Skin friction coefficient for (a) LST case; (b) LSHF case with $n_1=n_2=3$, $w_f=100\text{ gr}$, $Pr=2$ and $\varepsilon=M=1$



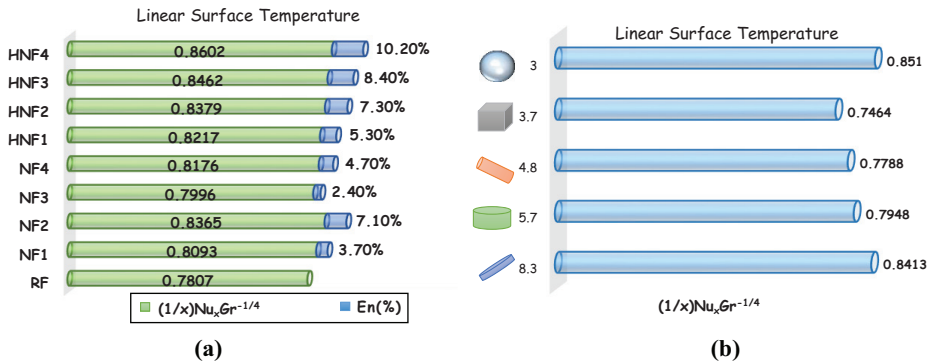
Source: Figure by authors

Table 7. The applied working fluids in the present study with abbreviations

Types	Description	w_1 (gr)	w_2 (gr)
RF	Regular fluid	0	0
NF1	Nanofluid (type 1)	15	0
NF2	Nanofluid (type 2)	30	0
NF3	Nanofluid (type 3)	0	15
NF4	Nanofluid (type 4)	0	30
HNF1	Hybrid nanofluid (type 1)	15	15
HNF2	Hybrid nanofluid (type 2)	15	30
HNF3	Hybrid nanofluid (type 3)	30	15
HNF4	Hybrid nanofluid (type 4)	30	30

Source: Table by authors

Figure 8. Nusselt number for (a) the various working fluids with augmentation percentage and (b) the different nanoparticles, with $n_1=n_2=3$, $w_f=100\text{ gr}$, $Pr=2$, $\varepsilon=M=1$ and $w_1=w_2=10\text{ gr}$



Source: Figure by authors

comparison with the thermal conductivity of graphene oxide. From Figure 8(a), the highest values of $(1/x)Nu_xGr^{-1/4}$ is calculated for HNF4 (0.8602) which shows a 10.2% increase in the Nusselt number.

Figure 8(b) depicts how the nanoparticle configurations affect the Nusselt number and consequently convective heat transfer coefficient changes. Among five instances of nanoparticle configurations of disc, platelet, cylinder, brick and sphere, the most elevated Nusselt number is connected to the spherical state of nanoparticles equal to 0.8413. An important point to note is that, in some already reported results, the highest values of the Nusselt number were not obtained by spherical nanoparticles. Although the present results do not refuse the former ones and the main reason for the matter is the different applied model of viscosity in this work.

5.3 Bejan number analysis

In this section, the problem of the electrically conducting hybrid nanofluid flow adjacent to a down-pointing rotating vertical cone in the presence of a transverse magnetic field is explored in the framework of entropy generation concepts. The entropy generation number N_G and the Bejan number Be for the various parameters are depicted in Figures 9(a,b), 10(a,b) and 11(a,b). In Figure 9(a,b), the entropy generation and Bejan number versus second nanoparticle (silver) mass w_2 for the various values of the magnetic parameter with considering two cases of LST and LSHF are depicted. From Figure 9(a), the entropy generation number enhances with the second nanoparticle. Besides, the magnetic parameter has a reducing effect on the entropy generation number for both cases of LST and LSHF. This shows to control the entropy generation by rotational flow on the surface of cone, the value of the magnetic interaction parameter should be decreased, which is an subject of interest in nuclear-MHD spinning body propulsion (Lee et al., 1993). Figure 9(b) demonstrates in both cases of LST and LSHF, the Bejan number has a decreasing manner with the second nanoparticle mass and also the magnetic parameter.

The entropy generation and Bejan numbers versus second nanoparticle (silver) mass w_2 for the various spin parameter with considering two cases of LST and LSHF have been plotted in Figure 10(a,b). Obviously, the entropy generation number enhances with the mass of silver nanoparticles, while the reverse trend is demonstrated for the Bejan number. Another result from Figure 10(a,b) is that the spin parameter of the cone has an augmenting effect on the entropy generation number and a decreasing effect on the Bejan number.

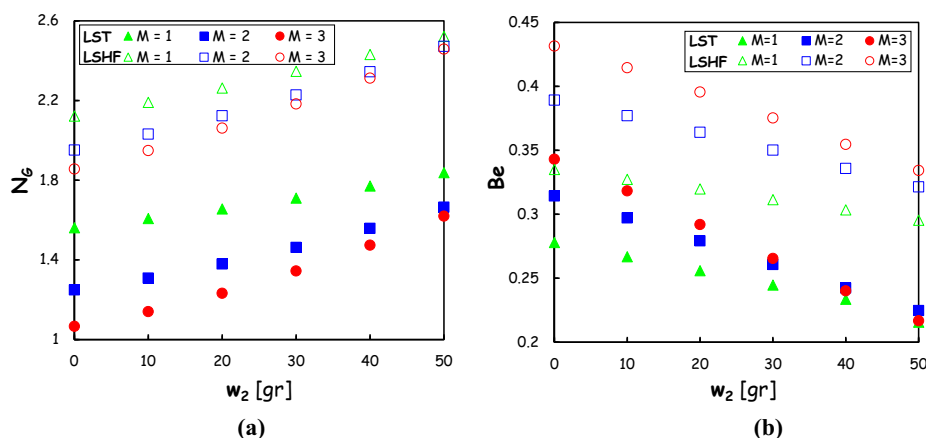


Figure 9. Effect of magnetic parameter on (a) entropy generation number and (b) Bejan number, for two cases of LST and LSHF, when $w_f = 100\text{ gr}$, $w_1 = 10\text{ gr}$, $n_1 = n_2 = 3$, $\varepsilon = 1$ and $Pr = 2$

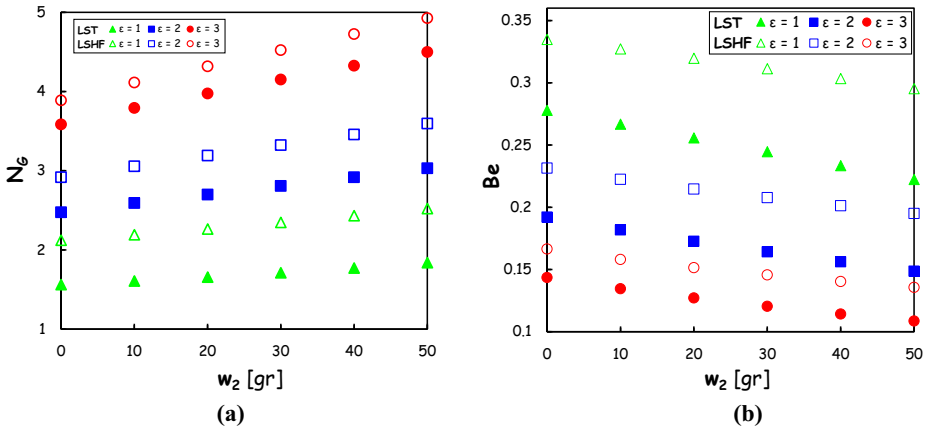
Source: Figure by authors

Figure 11(a,b) is plotted to demonstrate how the nanoparticle shape affects the generation of entropy and the Bejan numbers in two scenarios of LSHF and LST. The form of the particles affects how they move in a solid-liquid dispersion. Nonspherical particles in dispersions have greater difficulty rotating and translating than spherical nanoparticles do. The resistance to fluid flow is also greater in the presence of nonspherical particles than it is in the presence of spherical particles. Therefore, one can expect different results in the rheology of hybrid nanofluid for various shapes of nanoparticles. The spherical form of copper oxide and silver nanoparticles has the highest entropy generation value, while the cylindrical form has the lowest.

6. Final remarks

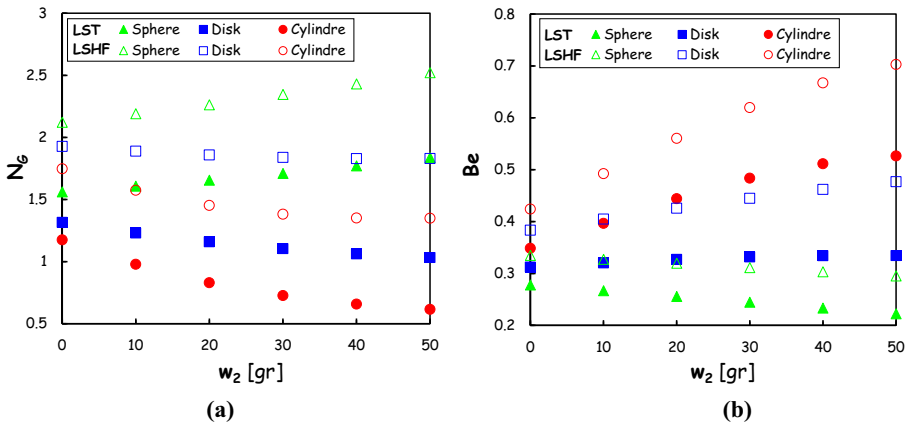
A numerical investigation has been done to analyze the free convective flow of a copper oxide-silver/water hybrid nanofluid adjacent to a down-pointing rotating vertical cone. The

Figure 10. Effect of spin parameter on (a) entropy generation number and (b) Bejan number, for two cases of LST and LSHF, when $w_f = 100\text{ gr}$, $w_1 = 10\text{ gr}$, $n_1 = n_2 = 3$, $M = 1$ and $Pr = 2$



Source: Figure by authors

Figure 11. Effect of nanoparticle shapes on (a) entropy generation number and (b) Bejan number, for two cases of LST and LSHF, when $w_f = 100\text{ gr}$, $w_1 = 10\text{ gr}$, $\epsilon = M = 1$ and $Pr = 2$



Source: Figure by authors

applied methodology is a combination of the Tiwari–Das nanofluid model and the mass-based algorithm to analyze the entropy generation and Bejan number for the first time. The mass-based algorithm uses the masses of base fluid (water) and nanoparticles (Ag and CuO) as an alternative to the first and second nanoparticles' volume fraction, according to the single-phase approach named the Tiwari–Das model (Dinarvand *et al.*, 2022b). The complicated basic PDEs are converted to non-dimensional form using the process of similarity transformation. These are solved by Runge–Kutta–Fehlberg approach combined with a shooting methodology for certain values of physical parameters. Subsequent to the fantastic compromise of the computational outcomes with past reports, the outcomes are introduced to conduct the investigation of the hydrodynamics/thermal boundary layers, the skin friction and the Nusselt number, as well as entropy generation and Bejan number. From results, the entropy generation number increases with the mass of the second nanoparticle in both LST and LSHF cases when the spherical shape of the nanoparticle is taken into consideration. It is worth mentioning that the combination use of the Tiwari–Das nanofluid model and the mass-based hybridity algorithm for the entropy generation analysis is the main novelty of this work. At long last, new demonstrating and approaches for the mixture nanofluid can be decisively helpful in the various applications in which the cooling advancements are fundamental.

References

- Afshari, F., Tuncer, A.D., Sözen, A., Variyenli, H.I., Khanlari, A. and Gürbüz, E.Y. (2021), “A comprehensive survey on utilization of hybrid nanofluid in plate heat exchanger with various number of plates”, *International Journal of Numerical Methods for Heat and Fluid Flow*, Vol. 32 No. 1, pp. 241-264.
- Agrawal, P., Dadheech, P.K., Jat, R.N. and Baleanu, S.D. (2021), “Radiative MHD hybrid-nanofluids flow over a permeable stretching surface with heat source/sink embedded in porous medium”, *International Journal of Numerical Methods for Heat and Fluid Flow*, Vol. 31 No. 8, pp. 2818-2840.
- Alarabi, T.H., Rashad, A.M. and Mahdy, A. (2021), “Homogeneous–heterogeneous chemical reactions of radiation hybrid nanofluid flow on a cylinder with joule heating: Nanoparticles shape impact”, *Coatings*, Vol. 11 No. 12, p. 1490.
- Bayram, M. and Ece, M.C. (2002), “Unsteady laminar boundary layer flow over a spinning body in free convection”, *Transactions of the Canadian Society for Mechanical Engineering*, Vol. 26 No. 1, pp. 121-135.
- Beg, O.A., Uddin, M.J., Beg, T. and Gorla, R.R. (2016), “Numerical simulation of self-similar thermal convection from a spinning cone in anisotropic porous medium”, *Journal of Hydrodynamics*, Vol. 28 No. 2, pp. 184-194.
- Bejan, A. (1979), “A study of entropy generation in fundamental convective heat transfer”, *Journal of Heat Transfer*, Vol. 101 No. 4, pp. 718-725.
- Berrehal, H., Dinarvand, S. and Khan, I. (2022), “Mass-based hybrid nanofluid model for entropy generation analysis of flow upon a convectively-warmed moving wedge”, *Chinese Journal of Physics*, Vol. 77, pp. 2603-2616.
- Chamkha, A.J. and Al-Mudhaf, A. (2005), “Unsteady heat and mass transfer from a rotating vertical cone with a magnetic field and heat generation or absorption effects”, *International Journal of Thermal Sciences*, Vol. 44 No. 3, pp. 267-276.
- Chandra Sekar Reddy, R., Reddy, P.S. and Sreedevi, P. (2022), “Impact of the Cattaneo–Christov heat flux on heat and mass transfer analysis of a hybrid nanofluid flow over a vertical cone”, *International Journal of Ambient Energy*, Vol. 43 No. 1, pp. 6919-6931.

- Devi, S.P.A. and Devi, S.S.U. (2016), "Numerical investigation of hydromagnetic hybrid Cu – Al₂O₃/water nanofluid flow over a permeable stretching sheet with suction", *International Journal of Nonlinear Sciences and Numerical Simulation*, Vol. 17 No. 5, pp. 249-257.
- Dinarvand, S. (2009), "A reliable treatment of the homotopy analysis method for viscous flow over a non-linearly stretching sheet in presence of a chemical reaction and under influence of a magnetic field", *Open Phys*, Vol. 7 No. 1, pp. 114-122.
- Dinarvand, S. and Mahdavi Nejad, A. (2022), "Off-centered stagnation point flow of an experimental-based hybrid nanofluid impinging to a spinning disk with low to high non-alignments", *International Journal of Numerical Methods for Heat and Fluid Flow*, Vol. 32 No. 8, pp. 2799-2818.
- Dinarvand, S. and Pop, I. (2017), "Free-convective flow of copper/water nanofluid about a rotating down-pointing cone using Tiwari-Das nanofluid scheme", *Advanced Powder Technology*, Vol. 28 No. 3, pp. 900-909.
- Dinarvand, S., Yousefi, M. and Chamkha, A.J. (2022a), "Numerical simulation of unsteady flow toward a stretching/shrinking sheet in porous medium filled with a hybrid nanofluid", *J. Appl. Comput. Mech*, Vol. 8 No. 1, pp. 11-20.
- Dinarvand, S., Berrehal, H., Khan, I. and Andualem, M. (2022b), "Mass-based hybrid nanofluid algorithm for entropy generation analysis of flow adjacent to a warmed and down-pointing rotating vertical cone", *Research Square*, doi: [10.21203/rs.3.rs-1444567/v1](https://doi.org/10.21203/rs.3.rs-1444567/v1).
- Dinarvand, S., Mousavi, S.M., Yousefi, M. and Nademi Rostami, M. (2022c), "MHD flow of MgO-Ag/water hybrid nanofluid past a moving slim needle considering dual solutions: an applicable model for hot-wire anemometer analysis", *International Journal of Numerical Methods for Heat and Fluid Flow*, Vol. 32 No. 2, pp. 488-510.
- Ece, M.C. (2001), "Free convection to power-law fluids from a vertical cone of variable surface temperature", *International Journal of Energy Research*, Vol. 25 No. 14, pp. 1221-1232.
- Ece, M.C. (2006), "Free convection flow about a vertical spinning cone under a magnetic field", *Applied Mathematics and Computation*, Vol. 179 No. 1, pp. 231-242.
- Ece, M.C. (1999–2000), "Free convection laminar boundary-layer flow of a power-law fluid about a vertical cone of variable surface heat flux", *J. Theor. Appl. Fluid Mech*, Vol. 2 No. 1, pp. 1-11.
- Hayat, T. and Nadeem, S. (2017), "Heat transfer enhancement with Ag–CuO/water hybrid nanofluid", *Results in Physics*, Vol. 7, pp. 2317-2324.
- Hoseinnejad, F., Dinarvand, S. and Yazdi, M.E. (2021), "Manninen's mixture model for conjugate conduction and mixed convection heat transfer of a nanofluid in a rotational/stationary circular enclosure", *International Journal of Numerical Methods for Heat and Fluid Flow*, Vol. 31 No. 5, pp. 1662-1694.
- Jaballah, R.B., HamidaSaleh, M.B.B.J. and Almeshaal, M.A. (2019), "Enhancement of the performance of bubble absorber using hybrid nanofluid as a cooled absorption system", *International Journal of Numerical Methods for Heat and Fluid Flow*, Vol. 29 No. 10, pp. 3857-3871.
- Jana, S., Salehi-Khojin, A. and Zhong, W.-H. (2007), "Enhancement of fluid thermal conductivity by the addition of single and hybrid nano-additives", *Thermochemical Acta*, Vol. 462 Nos 1/2, pp. 45-55.
- Lee, C.C., Jones, O.C. and Becker, M. (1993), "Thermofluid-neutronic stability of the rotating, fluidized bed, space-power reactor", *Nuclear Engineering and Design*, Vol. 139 No. 1, pp. 17-30.
- Li, Y., Shahsavari, A. and Talebizadehsardari, P. (2021), "Thermal conductivity of ethylene glycol-based nanofluid containing SiO₂ nanoadditives: experimental data and modeling through curve fitting", *Journal of Thermal Analysis and Calorimetry*, Vol. 146 No. 3, pp. 1101-1109.
- Mahian, O., et al. (2012), "Analysis of entropy generation between co-rotating cylinders using nanofluids", *Energy*, Vol. 44 No. 1, pp. 438-446.
- Mahian, O., et al. (2013), "A review of entropy generation in nanofluid flow", *International Journal of Heat and Mass Transfer*, Vol. 65, pp. 514-532.

- Menni, Y., Chamkha, A.G., Massarotti, N., Ameer, H., Kaid, N. and Bensafi, M. (2020), "Hydrodynamic and thermal analysis of water, ethylene glycol and water-ethylene glycol as base fluids dispersed by aluminum oxide nano-sized solid particles", *International Journal of Numerical Methods for Heat and Fluid Flow*, Vol. 30 No. 9, pp. 4349-4386.
- Ozturk, A. (2005), "Unsteady laminar mixed convection about a spinning sphere with a magnetic field", *Heat and Mass Transfer*, Vol. 41 No. 10, pp. 864-874.
- Ozturk, A. and Ece, M.C. (1995), "Unsteady forced convection heat transfer from a translating and spinning body", *Journal of Energy Resources Technology*, Vol. 117 No. 4, pp. 318-323.
- Ozturk, A. and Ece, M.C. (1999), "Buoyancy effects on unsteady laminar and rotational symmetric boundary layer", *Transactions of the Canadian Society for Mechanical Engineering*, Vol. 23 Nos 3/4, pp. 397-434.
- Ramzan, M., Shahmir, N., Alotaibi, H., Ghazwani, H.A.S. and Muhammad, T. (2022a), "Thermal performance comparative analysis of nanofluid flows at an oblique stagnation point considering Xue model: a solar application", *Journal of Computational Design and Engineering*, Vol. 9 No. 1, pp. 201-215.
- Ramzan, M., Gul, H., Ghazwani, H.A.S., Nisar, K.S., Abbas, M. and Saleel, C.A. (2022b), "Performance appraisal of Hamilton-Crosser and Yamada-Ota hybrid nanofluid flow models over a stretching cylinder with hall current and particle shape effectiveness", *International Journal of Modern Physics B*, Vol. 37 No. 10.
- Ramzan, M., Shahmir, N., Saleel, C.A., Kadry, S., Eldin, S.M. and Saeed, A.M. (2023), "Model-based comparison of hybrid nanofluid Darcy-Forchheimer flow subject to quadratic convection and frictional heating with multiple slip conditions", *Numer. Heat Transf. A*, pp. 1-21.
- Reddy, P.S., Sreedevi, P. and Chamkha, A.J. (2018), "MHD boundary layer heat and mass transfer characteristics of nanofluid over a vertical cone under convective boundary condition", *Propulsion and Power Research*, Vol. 7 No. 4, pp. 308-319.
- Reddy, P.S., Sreedevi, P. and Chamkha, A.J. (2023), "MHD convective flow of swcnts-water and mwcnts-water nanofluid over a vertical cone with thermal radiation and chemical reaction", *Journal of Porous Media*, Vol. 26 No. 7, pp. 7-68.
- Shaheen, N., Ramzan, M., Kadry, S., Abbas, M. and Saleel, C.A. (2023), "Unsteady ternary hybrid-nanofluid flow over an expanding/shrinking cylinder with multiple slips: a Yamada-Ota model implementation", *Nanotechnology*, Vol. 34 No. 36.
- Sheikholeslami, M. and Shamlooei, M. (2017), "Magnetic source influence on nanofluid flow in porous medium considering shape factor effect", *Physics Letters A*, Vol. 381 No. 36, pp. 3071-3078.
- Sidik, N.A.C., Jamil, M.M., Japar, W.M.A.A. and Adamu, I.M. (2017), "A review on preparation methods, stability and applications of hybrid nanofluids", *Renewable and Sustainable Energy Reviews*, Vol. 80, pp. 1112-1122.
- Sreedevi, P., Reddy, P.S. and Sheremet, M. (2020), "A comparative study of Al₂O₃ and TiO₂ nanofluid flow over a wedge with non-linear thermal radiation", *International Journal of Numerical Methods for Heat and Fluid Flow*, Vol. 30 No. 3, pp. 1291-1317.
- Takhar, H.S., Chamkha, A.J. and Nath, G. (2003), "Unsteady mixed convection flow from a rotating vertical cone with magnetic field", *Heat and Mass Transfer*, Vol. 39 No. 4, pp. 297-304.
- Tamim, H., Dinarvand, S., Hosseini, R., Khalili, S. and Pop, I. (2014), "Unsteady mixed convection flow of a nanofluid near orthogonal stagnation point on a vertical permeable surface", *Proc Inst Mech Eng Part E J Process Mech Eng*, Vol. 228 No. 3, pp. 226-237.
- Timofeeva, E.V., Routbort, J.L. and Singh, D. (2009), "Particle shape effects on thermophysical properties of alumina nanofluids", *Journal of Applied Physics*, Vol. 106, pp. 014304-014310.
- Tiwari, R.J. and Das, M.K. (2007), "Heat transfer augmentation in a two-sided lid-driven differentially heated square cavity utilizing nanofluids", *International Journal of Heat and Mass Transfer*, Vol. 50 Nos 9/10, pp. 2002-2018.

- Waini, I., Ishak, A. and Pop, I. (2021), "Hybrid nanofluid flow towards a stagnation point on an exponentially stretching/shrinking vertical sheet with buoyancy effects", *International Journal of Numerical Methods for Heat and Fluid Flow*, Vol. 31 No. 1, pp. 216-235.
- Yazdi, M.E., Moradi, A. and Dinarvand, S. (2014), "MHD mixed convection stagnation-point flow over a stretching vertical plate in porous medium filled with a nanofluid in the presence of thermal radiation", *Arabian Journal for Science and Engineering*, Vol. 39 No. 3, pp. 2251-2261.

Corresponding author

Saeed Dinarvand can be contacted at: saeed_dinarvand@yahoo.com or sae.dinarvand@iauctb.ac.ir